Magn Reson Mater Phy (2008) 21:187–196
DOI 10.1007/s10334-008-0110-x

RESEARCH ARTICLE

Automatic coil selection for channel reduction in SENSE-based parallel imaging

Mariya Doneva · Peter Börnert

Received: 6 August 2007 / Accepted: 4 March 2008 / Published online: 3 April 2008
© ESMRMB 2008

Abstract
Objective Coil arrays with large number of receive elements allow improved imaging performance and higher signal-to-noise-ratio. The MR systems supporting these arrays have to handle an increased amount of data and higher reconstruction burden. To overcome these problems, data reduction techniques need to be applied, realized either by linear combination of the original coil data prior to reconstruction or by discarding particular data from unimportant coil elements.
Materials and methods This work focuses on the latter approach and presents an efficient algorithm for automatic coil selection applicable to SENSE imaging. A singular value decomposition (SVD)-based coil selection is proposed that performs a coil element ranking quantifying the contribution of each coil element to the image reconstruction allowing appropriate coil selection. This approach makes use of the coil sensitivity information and takes reduction factor and phase encoding direction into account.
Results Simulations, phantom and in vivo experiments were performed to validate the SVD-based coil selection algorithm. The proposed approach proved to be computationally efficient without remarkable image quality degradation.
Conclusion The SVD-based approach offers the opportunity for fast automatic coil selection. This could simplify clinical workflow and may, furthermore, pave the way for various 2D real-time and interventional applications.

M. Doneva
University of Oldenburg, Oldenburg, Germany
e-mail: mariya.doneva@philips.com

P. Börnert (✉)
Philips Research Laboratories, Röntgenstraße 24-26,
23335 Hamburg, Germany
e-mail: peter.boernert@philips.com

Keywords MR imaging · Parallel MRI · RF coils · Coil selection

Introduction

Parallel imaging using coil arrays with a large number of independent coil elements provides improved imaging performance and increased signal-to-noise-ratio (SNR) [2,17,20,22]. Today, there is a fundamental trend to considerably increase the number of coil elements used for reception. Recently, 32-element coils [12,13,18] have been introduced to boost SNR and to allow for higher reduction factors. Even more complex coil arrays have been proposed and realized, consisting of up to 128 individual elements [4,8,15]. However, a number of these coil arrays have been used on systems supporting only 32 receive channels [21]. The use of a large number of coil array elements can lead to memory storage problems and to increased reconstruction times.

To overcome these problems, data reduction techniques could be applied. These can be realized by a linear combination of the original coil data prior to reception, using an appropriate hardware combiner [7,19], data compression of the sampled data before reconstruction [1,5], or by discarding particular data from coil elements with low signal content (either before or after reception) [9,11]. The concept of a hardware combiner for the realization of the linear combination of the coil signals was presented by King et al. [7] and Reykowski et al. [19].

Data compression can be based on the properties of the measured data, without the knowledge of the coil sensitivities. The software compression method, proposed by Huang et al. [5], applies principle component analysis for data reduction before the actual reconstruction. This data reduction strategy is appropriate for k-space based

reconstruction techniques [2,22], where the coil sensitivities are not known.

Buehrer et al. [1] presented a technique for coil array compression that finds an orthogonal space spanned by the totality of coil sensitivities and discards the unimportant directions in this space. The MR data can be projected to this lower dimensional space of virtual coils, balanced between all pixels in a defined region of interest (ROI). In this way, the number of "coils" used in the reconstruction can be decreased in a preprocessing step without significant loss of SNR.

For the situation of a limited number of channels, a greater number of available receive coils and no hardware-based signal combination, a selection rule is needed to find the coil element configuration leading to optimal image quality. The coil elements used could either be a fixed set of individual coils, optimal for a given measurement, or could be dynamically selected during the image acquisition satisfying a local optimality criterion. On the other hand, such coil selection could also be used prior to the image reconstruction to reduce the reconstruction time, which is important for real-time imaging applications.

The dynamic coil selection (DCS) algorithm, proposed by Mueller et al. [11], selects a subset of receive coils to reduce the image reconstruction time in interventional imaging. This algorithm performs coil ranking based on two criteria: (i) the distance between the location with highest sensitivity for each coil and the current slice and (ii) the signal intensity in each coil. The algorithm is simple and thus allows for fast coil selection, but this choice of coil elements might be suboptimal for acceleration factors greater than one, since no optimization for parallel imaging is included.

The method presented in this work reduce the dimensionality of the problem by discarding the data from the least important coils. An algorithm for automatic coil selection applicable to SENSE imaging is presented. The decision rules applied are related to the noise propagation in parallel imaging; thus, the coil selection depends on the particular parallel imaging conditions like reduction factor and phase encoding direction. The singular value decomposition (SVD)-based coil element selection is described and evaluated, based on simulated, phantom and in vivo data.

Methods

Theory

Coil element selection refers to dimensionality reduction, in which an optimal subset of physical or virtual coils is selected for image reconstruction. In principle, it is necessary to consider all possible subsets, since combinations of variables can provide significant information which is not available in any of the individual variables separately. With an increasing number of available coils, however, the number of possible subsets grows very rapidly and an exhaustive search becomes unpractical.

Another possibility is to preprocess the data and to select variables according to heuristics, based on general characteristics of the data, such as orthogonality and high information content. This approach usually runs much faster, because no explicit search is needed. However, it could lead to suboptimal results.

SVD-based coil selection

SENSE reconstruction of uniformly undersampled Cartesian data consists of solving a linear system of L equations with R variables, where L is the number of coil elements, and R is the reduction factor. The R unknowns could be uniquely determined if they were measured with a basis of R orthogonal coils. Solving this system of equations could be presented as projecting the problem from the L to the R dimensional space and then solving it in the lower dimensional space.

Ohliger et al. [14] proposed a method to estimate the ultimate SNR for parallel imaging by successively adding plane wave modes until SNR saturation, such that the coil sensitivity functions that were added up to this point, build an ideal basis for solving the reconstruction problem. This basis can be used as a measure for the ultimate SNR.

In a similar way, if the best subset of a given coil set has to be selected, the upper SNR limit would be given by the full coil set. Finding those coils that have the most similar projection of the R dimensional problem space to the projection of the full coil set will result in an optimal SNR coil configuration of the given size. Based on this idea, a selection method is presented using the SVD factorization [16] of the sensitivity matrices and will be, therefore, denoted as the SVD-based coil selection method.

Consider a SENSE reconstruction problem with Cartesian k-space sampling at a reduction factor R in an arbitrary direction [17] using an L-element coil array. The reconstruction problem at each pixel is given by:

$$\mathbf{a} = \mathbf{S}\mathbf{b} + \mathbf{n}. \tag{1}$$

The vector $\mathbf{a}$ consists of the complex pixel intensities in the reduced field of view (FOV) images for each coil, $\mathbf{S}$ is the $L \times R$ sensitivity matrix, $\mathbf{b}$ is a vector containing the original image pixels, which are superimposed in the aliased images, and $\mathbf{n}$ is a noise vector. The reconstruction consists of solving the linear system of (1) for each aliased pixel in the reduced FOV. This system is overdetermined; thus, an estimation technique has to be used for finding the solution. Assuming Gaussian statistics for the noise, the best linear unbiased estimator (BLUE) [10] of vector $\mathbf{b}$ is given by:

$$\mathbf{b} = \left(\mathbf{S}^H \Psi^{-1} \mathbf{S}\right)^{-1} \mathbf{S}^H \Psi^{-1} \mathbf{a}, \tag{2}$$

where Ψ is the $L \times L$ receiver noise covariance matrix, which helps to optimize SNR during the reconstruction. The noise covariance matrix may be replaced by an identity matrix, leading to the least squares estimator for $\mathbf{b}$. In this case, the unfolding is still ensured, yet at an SNR penalty, which will be the more significant, the less equivalent the receivers are with respect to load, gain, and mutual coupling.

Alternatively, matrix factorization techniques might be used to obtain the linear least squares solution in a numerically stable fashion. The most common matrix factorization technique used for solving an overdetermined system of linear equations is the SVD [16].

Using SVD, the sensitivity matrix $\mathbf{S}$ can be factorized as $\mathbf{S} = \mathbf{U}\Sigma\mathbf{V}^H$, and the SVD solution of (1) is given by:

$$\mathbf{b} = \mathbf{V}\Sigma^{+}\mathbf{U}^H\mathbf{a}, \tag{3}$$

where Σ^+ is the transposed of Σ with every value, greater than a preset threshold, replaced with its reciprocal.

Equation (3) can be written in the form:

$$\mathbf{U}^H\mathbf{a} = \mathbf{U}^H\mathbf{S}\mathbf{b} = \Sigma\mathbf{V}^H\mathbf{b} \tag{4}$$

considering only the rows of $\mathbf{U}^H$, Σ, and $\mathbf{V}$ corresponding to singular values greater than the threshold. The matrix $\mathbf{U}^H$ projects both the data and the sensitivity matrix into lower dimensional space, corresponding to the rank of the matrix $\mathbf{S}$. Let us denote this projection of the coil sensitivity matrix with $\mathbf{S}'$, the corresponding projection of the data vector with $\mathbf{a}'$ and the projection matrix, which transforms $\mathbf{S}$ to $\mathbf{S}'$ with $\mathbf{P}$, where $\mathbf{P} = \mathbf{U}^H$.

$$\begin{aligned} \mathbf{a}' &= \mathbf{U}^H\mathbf{a} = \mathbf{P}\mathbf{a} \\ \mathbf{S}' &= \mathbf{U}^H\mathbf{S} = \mathbf{P}\mathbf{S}. \end{aligned} \tag{5}$$

The rows of the new sensitivity matrix $\mathbf{S}'$ can be considered as sensitivities of a set of virtual coils, which sensitivity vectors are obtained as a superposition of the real physical coil sensitivities. The coils can be ranked according to their relative contribution to the virtual coils. The ith row vector of $\mathbf{S}'$ can be written as a linear combination of the rows of $\mathbf{S}$

$$\mathbf{s}'_{\mathbf{i}} = \sum_k p_{ik}\mathbf{s}_{\mathbf{k}}, \tag{6}$$

where the weighting factors $\mathbf{P}(i,k) = p_{ik}$ $(k = 1, \ldots, n_c)$ are the ith row entries of matrix $\mathbf{P}$. The magnitude of p_{ik} represents the contribution of the kth physical coil to the ith virtual coil. In this way, the coil array elements can be ranked according to the weighting function:

$$w_k = \sum_i |p_{ik}|. \tag{7}$$

The weighting function can be calculated for each reconstructed pixel in the full FOV image or for a given ROI, and the optimal coil set is chosen according to the total weight for this region.

$$W_k = \frac{\sum_{\mathbf{r}\in ROI} w_k(\mathbf{r})}{N_{ROI}}. \tag{8}$$

In this way, a single step coil selection is performed using the SVD of the sensitivity matrix.

To validate the performance of the method, it should be compared with the results of the exhaustive search through all possible coil sets that determines the optimal coil set in SNR sense. However, the number of possible coil combinations makes this task impossible. A faster search using a sequential backward elimination [3] allows the selection in manageable times. We will denote this algorithm as the SNR-based coil selection method and will use it as a reference.

SNR-based coil selection with sequential backward elimination search

In the context of coil element selection, an appropriate criterion (or cost function) should refer to the image quality if the image acquisition is performed with a given coil configuration. One of such quality measures is the SNR.

Unlike in conventional Fourier MRI, the transforms used in sensitivity encoded image reconstruction are generally not unitary, and spatially variable noise amplification occurs [14, 17]. As a result, the SNR is also variable over the FOV. For the SNR at position $\mathbf{r}_n$ holds [14]:

$$\mathrm{SNR}(\mathbf{r}_n) \propto \frac{1}{\sqrt{\mathbf{X}_n}}, \tag{9}$$

where $\mathbf{X}_n$ is the total noise power at pixel position $\mathbf{r}_n$, which in the case of regular Cartesian sampling is given by [17]:

$$\mathbf{X}_n = \frac{1}{N_x N_y}[(\mathbf{S}^H\Psi^{-1}\mathbf{S})^{-1}]_{nn}, \tag{10}$$

where $\mathbf{S}$ is the sensitivity matrix, Ψ is the receiver noise matrix, and $N_x N_y$ denotes the number of samples acquired in the k-space. The SNR is, therefore, proportional to the following:

$$\mathrm{SNR}(\mathbf{r}_n) \propto \frac{\sqrt{N_x N_y}}{\sqrt{[(\mathbf{S}^H\Psi^{-1}\mathbf{S})^{-1}]_{nn}}}. \tag{11}$$

The expression on the right-hand side represents the SNR dependency on the reconstruction and will be further denoted as the SNR-factor. The SNR in parallel imaging is spatially variable, so optimizing the local SNR-factor will lead to a different coil configuration for each pixel. A better approach would be to consider a global value, such as the mean SNR-factor, for the decision.

Another characteristic of the image quality is the smallest value of the SNR in the reconstructed image; thus, considering only the pixels within a given ROI, or the fraction of

the pixels with lowest SNR-factor may lead to a better selection criterion than averaging over the complete FOV. The cost function, determined by the mean SNR-factor over a selected ROI is given by:

$$J(X_l) = \frac{\sum_{\mathbf{r}_i \in \mathrm{ROI}} \text{SNR-factor}(\mathbf{r}_i)}{N_{\mathrm{ROI}}}, \tag{12}$$

where N_{ROI} denotes the number of samples in the ROI. The SNR criterion is used together with the sequential backward elimination search technique for coil element selection. This SNR-based coil selection method represents the "gold standard" in this work that will be used to evaluate feasibility of the SVD-based coil selection.

In the two coil selection algorithms described here, derived for Cartesian sampling of k-space, the cost function is initially calculated on a pixel basis, and then a global decision is made using a mean cost function for a given ROI. Alternatively, an average reconstruction problem might be considered, like the one proposed by Buehrer et al. [1], and then a single value for the cost function would be obtained.

The fact that coil sensitivities vary slowly over the FOV allows further acceleration of the selection algorithms, by considering only a subset of the coil sensitivity values for the selection.

The SVD-based coil ranking evaluates the contribution of each individual coil to the full coil set at a single step; thus, it performs a fast decision, but may lead to suboptimal results, because it does not take the group performance into account. The SNR-based coil selection takes into account the group performance of the considered coil sets, but requires multiple evaluations of coil sets and, therefore, more time for reaching a decision.

It is important to note, that the coil selection process can be locally optimized. This can mean that in a 2D case optimization is restricted only to a part of the FOV, whereas in 3D or multi-slice imaging the selection can be performed, e.g., for each individual slice.

Experimental

The SVD-based coil selection algorithm was evaluated on the basis of simulated data as well as phantom and in vivo measurements.

Simulations

One hundred different sets of computer generated coil sensitivity maps were used in the simulation, while each set consisted of 32 coil elements. The coil array elements were modeled as circular coils with 40 mm radius. The coil element positions were randomly chosen within the area constraint by two coaxial cylinders, whereas their orientation was chosen tangentially to the cylinders (Fig. 1). By using this approach simple wraparound coils were modeled. Sensitivity maps were calculated using the Biot–Savart law for a 384 × 384 pixel matrix and FOV 384 × 384 mm^2 arranged as a plane, orthogonal to the cylinder axis. The radii of the cylinders were chosen to be $r = 271.5$ and $R = 300$ mm such that all coils lie outside the FOV. In the z direction, the coil positions vary between −200 and 200 mm from the considered FOV.

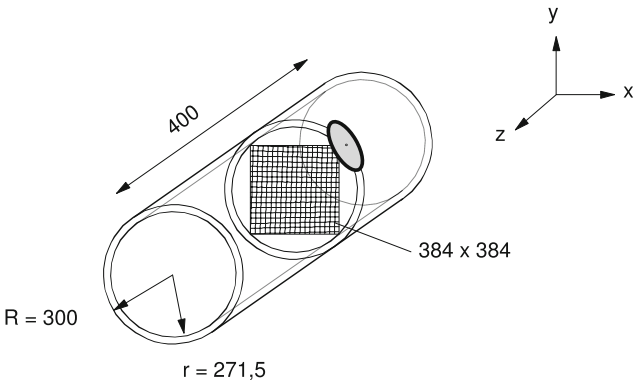

Fig. 1 Simulation setup. Coil element positions were randomly chosen within the two coaxial cylinders with radii 271.5 and 300 mm and length of 400 mm, oriented tangentially to the cylinder. Sensitivity maps were calculated for a 384 × 384 matrix arranged as a plane, orthogonal to the cylinder axes. A sample coil element shown schematically

The SENSE direction was assumed to be along the y axis using a reduction factor of $R = 2$. The SVD-based and the SNR-based coil selection methods were compared in the task of choosing the optimal 16 out of 32 coil elements. The specific choice of the ROI used for the coil selection is problem dependent and could be a subject of further optimization.

In the current simulation, first an SNR-factor evaluation was performed for the full coil set, and a mask was formed choosing the 25% of pixels having a lowest SNR-factor.

$$m_{25}(\mathbf{r}_i) = \begin{cases} 1 \text{ if } \text{SNR-factor}(\mathbf{r}_i) < Q_1(\text{SNR-factor}) \\ 0 \text{ else} \end{cases}, \tag{13}$$

where $m_{25}(\mathbf{r}_i)$ denotes the value of the mask at position $\mathbf{r}_i$, and Q_1(SNR-factor) is the first quartile of the SNR-factor.

For each of the 100 cases, a list of the 16 coils selected from each of the two coil selection algorithms was obtained. The results from the SNR-based and the SVD-based coil selection methods were compared on the basis of the mean SNR-factor in the potential images, reconstructed with the chosen coil sets

$$\mu_{25} = \frac{\sum_i \text{SNR-factor}(\mathbf{r}_i) m_{25}(\mathbf{r}_i)}{\sum m_{25}(\mathbf{r}_i)}. \tag{14}$$

The ratio of the mean SNR-factor for the two decision cases

$$q = \frac{\mu_{25}(\text{SVD selection})}{\mu_{25}(\text{SNR selection})} \tag{15}$$

is additionally considered as a comparison measure.

To understand the effect of the coil selection on the pixels that were not included in the selection algorithms, the evaluations of the mean SNR-factor and the ratio q were also performed on the complete FOV.

Phantom and in vivo measurements

All measurements were made on a clinical scanner operating at 1.5T (Achieva, Philips Medical Systems). RF transmission was performed using the homogeneous RF body coil, while a 32-element coil array, which was designed for cardiac applications, was employed for signal reception. The coil array consists of two independent parts, an anterior and a posterior part, each composed of 16 hexagonal receive coil elements with 60 mm edge length [23]. While exhibiting a slightly different coil element arrangement, both parts basically consist of three rows of elements in feet-head (FH) direction, each composed of 5–6 elements in left–right (LR). With the anterior and posterior part in place the entire coil arrangement has a FH/LR coverage of 270/540 mm, respectively. The anterior coil is flexible and can be bent around the patient for an optimal coverage. The posterior part has a prebent structure in LR direction and is fixed to the patient table.

Phantom measurements The 2D images of the phantom were acquired using a steady state free precession sequence with balanced gradients (balanced FFE, true FISP) with TE = 1.5 ms, TR = 3 ms, flip angle $\alpha = 60°$, FOV = 410 × 410 mm^2, matrix size 288 × 288 pixels and slice thickness of 7 mm, $R = 2$ in anterior–posterior (AP).

In vivo measurements In vivo measurements were performed on five healthy volunteers (two for the 2D and three for the 3D measurements), after informed consent obtained. The 2D abdominal data were obtained using the same imaging protocol as in the phantom measurement. Additionally, 3D pelvis measurements were performed with TE = 2 ms, TR = 4 ms, balanced FFE, flip angle $\alpha = 50°$, FOV = 450 × 450 × 192 mm^3, matrix size 192 × 192 × 48 voxels $R = 6$ (2 in AP and 3 in FH).

To quantify the experimental results, SNR evaluations were performed. Precise SNR measurement for parallel imaging is not trivial, since the SNR varies within the FOV and background noise estimation is often difficult [6]. To circumvent this and to give experimental values, a very simple SNR measure was chosen. This was defined as the ratio of the mean and the standard deviation of the MR signal in homogeneous regions (100 pixels) in the reconstructed images. To get a more global measure, the average was formed over several (5–6) spatially distant regions of similar signal amplitude. Although this is a rather rough measure, it shows the relation between the different coil configurations, since this SNR evaluation is performed at the same locations for a given scan. Additionally, the mean SNR-factor, which is based on the coil sensitivity information was calculated for comparison.

Results

Simulation

Figure 2a shows the scatter plot of the mean SNR-factor according to (14) for the pixels that were used for coil selection. The mean SNR-factor is very well correlated between the two algorithms for all 100 simulated data sets. The histogram of q (Fig. 2b) shows that both algorithms lead to the same result in almost half of the cases, while the SNR loss due to suboptimal decision of the SVD-based algorithm is

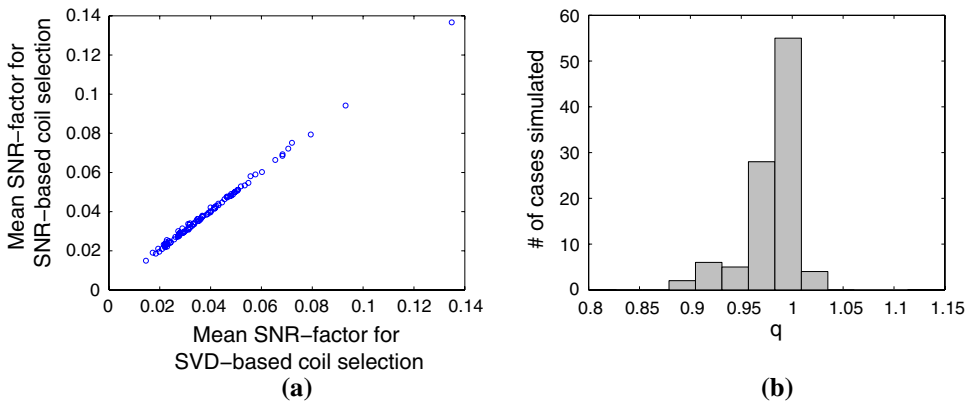

Fig. 2 Comparison between SVD-based and SNR-based coil selection algorithms. The ROI, used for coil selection was defined by the 25% of the data with lowest SNR in the FOV. This evaluation is based on the mean SNR-factor on the ROI used for coil selection. **a** Scatter plot of the mean SNR factor for the coil configurations selected by the SNR-based and SVD-based coil selection. **b** Histogram of the ratio of the mean SNR-factor for the coil configuration found by the two different approaches (q)

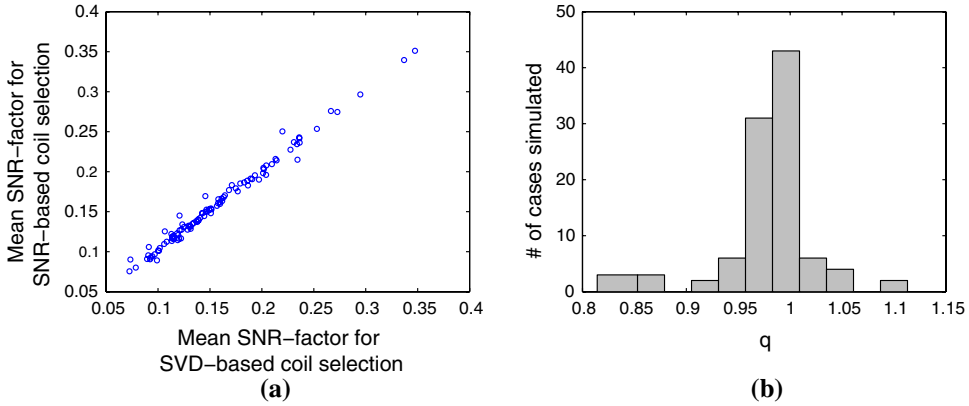

Fig. 3 Comparison between SVD- and SNR-based coil selection algorithms. The same coil element selection underlying the analysis shown in Fig. 2 is here evaluated on the complete FOV. **a** Scatter plot of the mean SNR for the coil configurations selected by the SNR-based and SVD-based coil selection. **b** Histogram of the ratio q of the mean SNR-factor for the coil configuration found by the SVD- and SNR-based selection algorithms for 100 simulation sets. Compared with Fig. 2, this distribution includes values greater than one and shows a higher mean value and standard deviation

not more than 10% in the other cases. The mean value of the given distribution $\mu(q) = 0.982$, and the standard deviation $\sigma(q) = 0.025$. Thus, the mean SNR loss in the decision ROI for coil configuration chosen with the SVD-based selection, compared with the SNR-based selection, was less that 2% for the 100 simulation sets.

Figure 3a shows the scatter plot of the mean SNR-factor for the same selected coil sets, evaluated on the entire FOV. Again, the mean SNR-factor for the two algorithms shows very good correlation. The ratio q of the mean SNR-factor for the two selections has a greater variance for the complete FOV $\sigma(q) = 0.044$, which could be explained by the inclusion of pixels that were not used in the coil selection. However, the mean value $\mu(q) = 0.985$ is slightly increased in this case.

The results of the simulations show that the SVD-based coil selection method gives comparable results to the SNR-based selection at greatly reduced computational complexity. Additionally, single coil set evaluation requires more calculations for the SNR-based coil selection than for the SVD-based selection, which leads to an even greater factor for the required computation times. The computation time for a 384×384 matrix was evaluated on a Xeon processor, CPU 2.4 GHz, 4 GByte memory. The time for the SVD-based coil selection was $t_{\mathrm{svd}} = 0.02$ s, and the time for the SNR-based coil selection was $t_{\mathrm{snr}} = 16.3$ s, which is far too long for the clinical practice. For further evaluation, the algorithms were applied on phantom and in vivo data.

Phantom measurements

Figure 4a and b show the images obtained with 16 coils selected with the SVD-based and SNR-based coil selection algorithms, respectively. These images were taken in the transverse plane with reduction a factor $R = 2$ in AP direction and were reconstructed using SENSE. In both cases, only pixels within the object were included in the decision algorithm. For both algorithms, the images, reconstructed with the reduced coil sets, show only a small decrease in SNR compared with the image obtained with the full set of 32 coils (Fig. 4c). In comparison, a rather high noise level is visible in the image reconstructed from the 16 coils that were eliminated by the SVD-based coil selection (Fig. 4d). The mean SNR-factor and mean measured SNR value are summarized in Table 1. The mean measured SNR was evaluated in the regions indicated on Fig. 4c. The selected coil set configuration is shown for each case on the coil geometry diagrams below each image. The slice position is indicated by the arrows leftmost coil geometry diagram.

In vivo measurements

Figure 5a and b show the 2D images (SENSE $R = 2$ in AP), reconstructed with 16 coil elements selected with the SVD- and SNR-based coil selection algorithms, respectively. In this case, again, both algorithms yield similar results with respect to coil selection, and no visible decrease in image quality is observed in comparison with the total coil set image (Fig. 5c). Figure 5d shows the image reconstructed from the 16 coils rejected by the SVD-based algorithm, which is again clearly noisier.

Figure 6a and b show a single slice from 3D image data (central transversal slice), reconstructed with 16 coil elements selected with the SVD- and the SNR-based coil selection algorithms from the undersampled data (SENSE $R = 6$). The coil selection was performed for the entire measured 3D volume. The two algorithms lead to similar coil selection patterns, evenly distributed between the anterior and

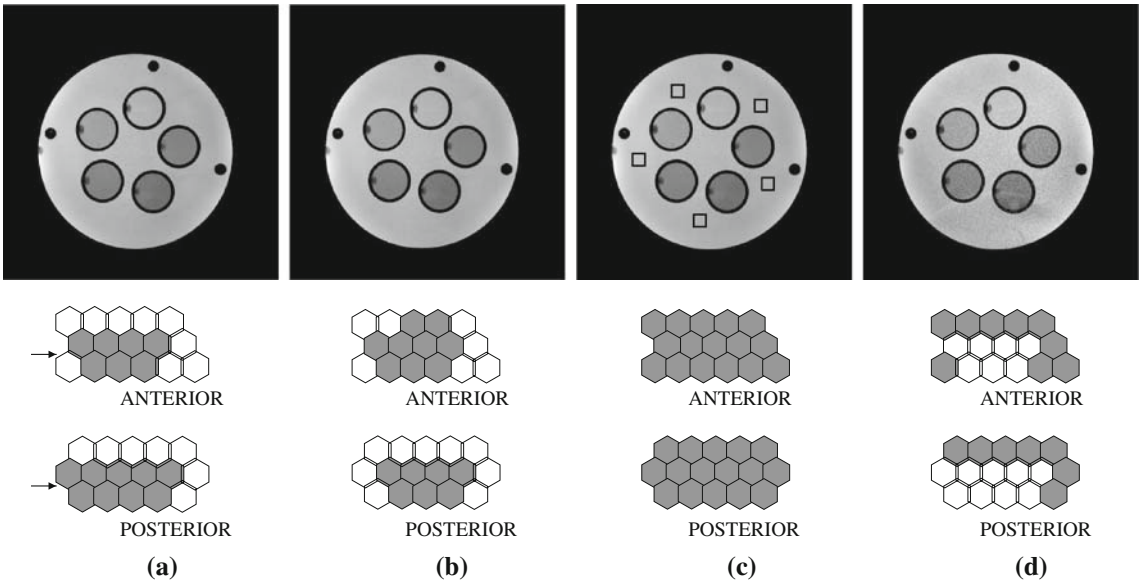

Fig. 4 Phantom experiments (16 out of 32). Images, reconstructed with **a** 16 coils chosen with the SVD-based coil selection algorithm, **b** 16 coils chosen with the SNR-based coil selection algorithm, **c** the full set of 32 coil elements and **d** the 16 coils eliminated by the SVD algorithm. The two different coil selection approaches lead to quite similar coil selection patterns as shown on the coil geometry diagrams below the images. The images, reconstructed with the coil subsets, selected by the two coil selection algorithms does not show a visible decrease in image quality, compared to the full 32 coil set image. In contrast, in the central part by the SVD-rejected image, a very high noise level is visible. The slice position is indicated by the *arrows* in the anterior and posterior part of the coil in the *leftmost diagram*. The 10 pixel regions used for SNR evaluation are indicated on the full coil set image (**c**)

Table 1 Mean SNR comparison

	Mean SNR-factor			Mean measured SNR		
	SNR	SVD	Full coil set	SNR	SVD	Full coil set
Phantom 2D	8.77	8.73	9.29	62.13	62.76	64.55
In vivo 2D	10.35	10.20	11.42	10.9	10.9	11.0
In vivo 3D	9.53	9.41	10.92	16.8	17.5	19.4

Mean SNR-factor and mean measured SNR values for the images, reconstructed with 16 out of 32 coils, selected with SNR-based, SVD-based coil selection and the full coil set of 32 elements, respectively

posterior part. SNR was measured and averaged over three distant slices of the 3D data. In Fig. 6c the selected regions for the given slice are indicated. The mean SNR-factor and mean measured SNR values obtained are given in Table 1. Applying higher reduction factors and measuring larger volumes limit the number of coils that can be eliminated without compromising the quality of the SENSE reconstruction. Although for most of the images in the 3D set a good quality was achieved with the reduced coil set, in some of the slices residual aliasing artifacts were present. This is illustrated in Fig. 7 that shows a different slice of the data shown in Fig. 6. The aliasing artifact, indicated by the arrows in Fig. 7a and b comes mainly from the FH direction due to incomplete unfolding.

Performance can be improved by performing coil selection locally for each slice, including only the locally optimal coil data in the reconstruction. As shown in Fig. 7c and d, local optimization leads to improved image quality in the chosen region, but could compromise image quality outside this area. This local coil selection in 3D is only applicable if all coil data have been measured. It helps to improve image quality and reduces reconstruction time, but does not ease the memory problem. The decision which coils should be used for which slice can quickly be obtained in advance or during the scan.

The decision time needed by the SVD-based coil selection for full 3D optimization was $t_{\mathrm{svd}} = 0.52$ s. The SNR-based coil selection needed about 5 min. The time necessary to select the optimal elements for a single slice out of the locally optimized decision time was $t_{\mathrm{svd}} = 0.08$ s for the SVD-based coil selection and $t_{\mathrm{snr}} = 22.7$ s for the SNR-based coil selection.

Discussion

Coil element selection could be a useful approach to cope with increasing system demands in future parallel MRI. In this work, an effective coil selection algorithm was presented, and its basic feasibility was demonstrated for two and three dimensional Cartesian imaging with various reduction factors.

Leaving out data of insensitive elements could be advantageously in practical situations. A low coil sensitivity could be a physical fact, e.g., proximity reasons, but could also be an

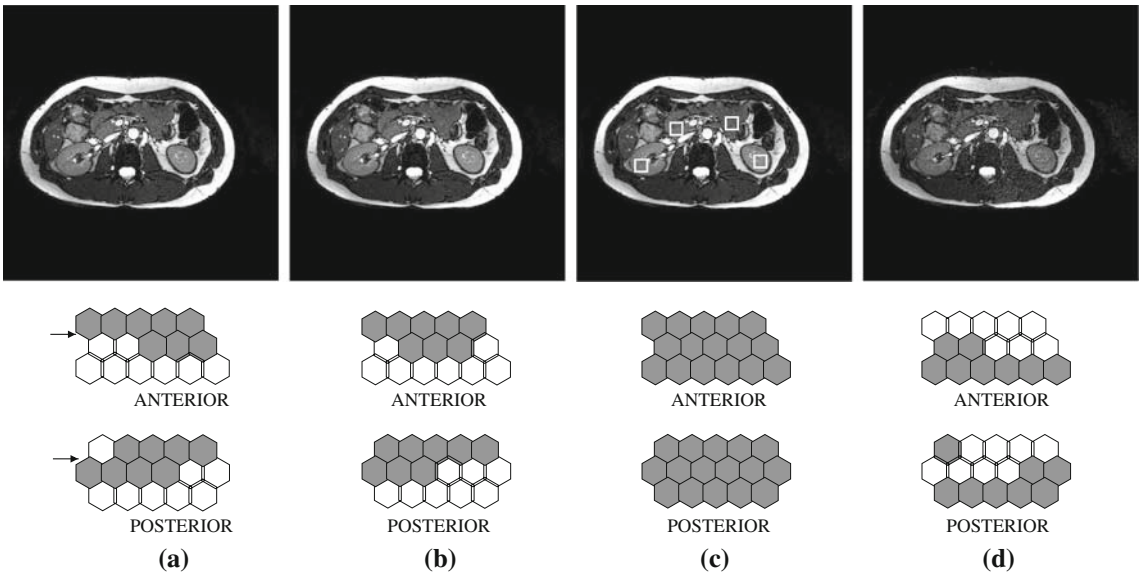

Fig. 5 In vivo results (16 out of 32). Images reconstructed with **a** 16 coils selected with the SVD-based coil selection algorithm, **b** 16 coils selected with the SNR-based coil selection algorithm, **c** the full set of 32 coils, **d** 16 coils rejected by the SVD coil selection algorithm. The selected coils are shaded in the coil array geometry diagram below each image and the slice position is indicated. The two algorithms show only small differences in the selected coils. The resulting 16-coil element images (**a**, **b**) are similar and do not show a visible decrease in SNR compared to the full coil set image (**c**). In comparison, the image reconstructed with the 16 coils, rejected by the SVD algorithm is visibly noisier (**d**). The *white squares* in **c** indicate the regions used for SNR evaluation

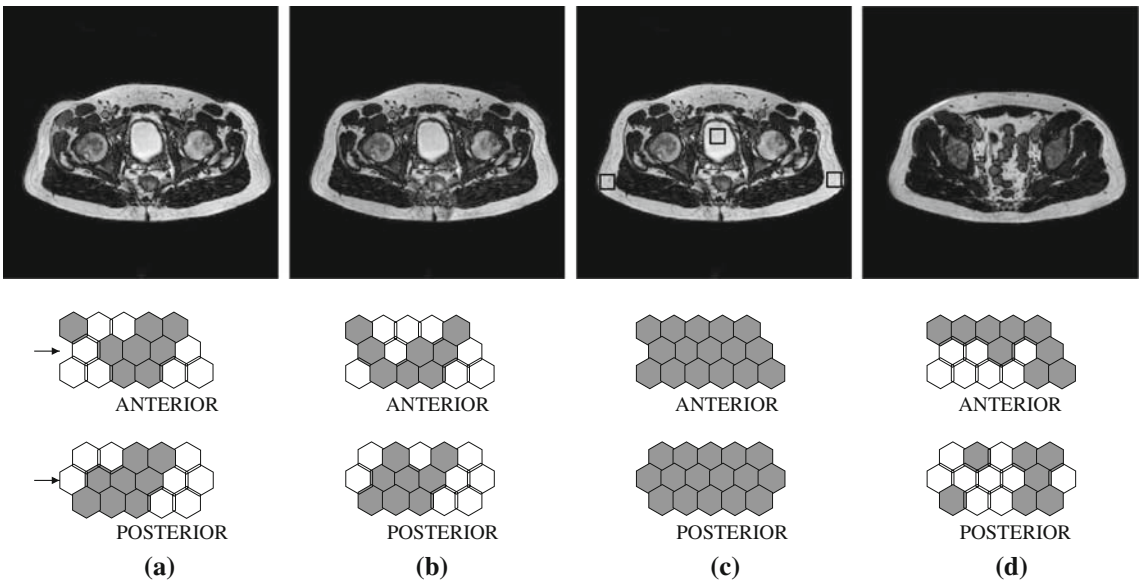

Fig. 6 In vivo results (16 out of 32). A transversal slice extracted from 3D data reconstructed with **a** 16 coils selected with the SVD-based coil selection algorithm, **b** 16 coils selected with the SNR-based coil selection algorithm, **c** the full set of 32 coils, **d** 16 coils rejected by the SVD coil selection algorithm. The selected coil elements and the slice position are marked on the coil array geometry diagrams. The two algorithms show only small differences in the coil selection. The resulting images (**a**, **b**) are similar and do not show a visible decrease in SNR compared to the full coil set image (**c**). The image of the SVD rejected coils shows residual aliasing artifacts (**d**). The regions used for SNR estimation in this slice are indicated on the image (**c**)

indication for a non-properly operating coil element. Those elements could be malfunctioning giving rise to serious noise or spike propagation into the final images, and it would be reasonable to exclude them in the image generation process. Coil element elimination could also be applied after digitization to decrease the reconstruction time [11]. Also in this case, the SVD-based coil selection would be an appropriate selection method, because of its short decision times.

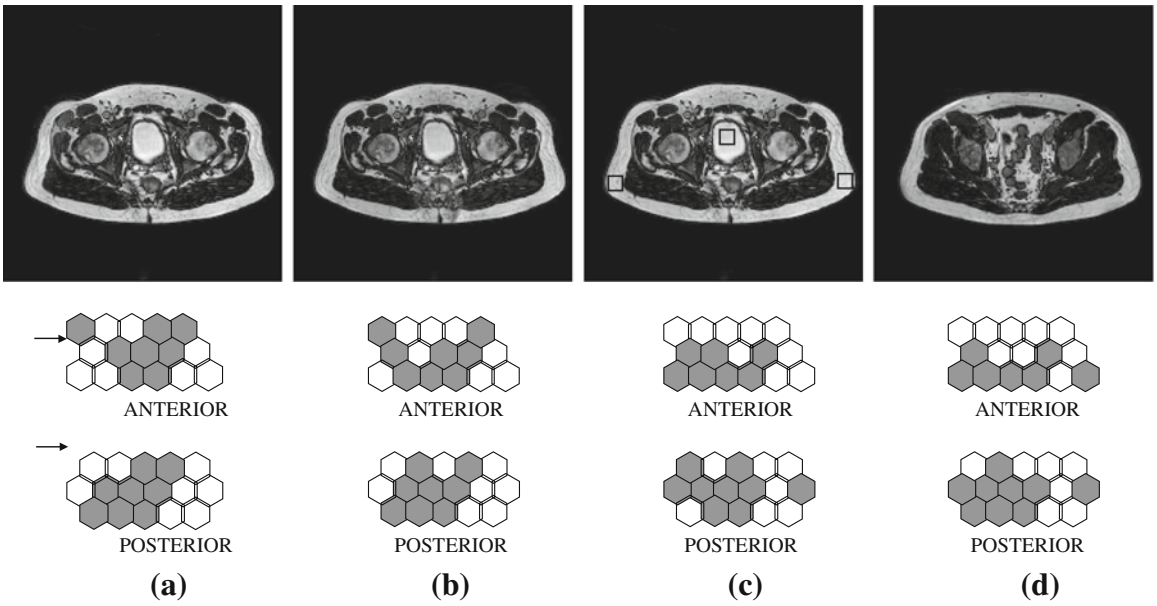

Fig. 7 In vivo results (16 out of 32). A transversal slice extracted from the same 3D data shown in Fig. 6 at different slice position. Images, reconstructed with (**a**) 16 coils selected with the SVD-based coil selection algorithm (**b**) 16 coils selected with the SNR-based coil selection algorithm show residual fold-over artifacts (indicated by the *arrow*). The same slice, reconstructed with the 16 coils, selected using local optimization (**c**) using the SVD-based coil selection and (**d**) using the SNR-based coil selection show improved image quality

Simulations, phantom and in vivo measurements were performed to evaluate the SVD-based coil selection method by comparing it to the more intuitive SNR-based coil selection. The phantom and in vivo measurements confirmed the results from the simulations that the two coil selection algorithms lead to comparable results. This is also shown by the SNR measures for the two selection algorithms summarized in Table 1. The measured SNR shows very good correspondence to the SNR-factor, theoretically derived from the coil sensitivities. The slightly higher measured SNR-values for the SVD-based selection approach are potentially caused by the limited accuracy of the SNR measure chosen and are considered to be non-significant. Due to its lower computational complexity, the SVD-based coil selection algorithm needed much lower computation times. This approach could further be improved by incorporating the noise correlation in the coil ranking, which was not considered in the present paper.

However, there are also some limitations. In 3D imaging extensive coil elimination might potentially compromise image quality, especially in highly accelerated scans. In that aspect a local coil selection can help to find an appropriate compromise. On the other hand, coil element elimination can be very advantageous if the coil array coverage is much larger than the actual FOV that one is interested in, which can be the case in many 2D applications, including multi-slice imaging. A local coil selection in the latter case allows dynamical coil switching, using the optimal coil subset for each slice, which could decrease the required memory storage and speed up the reconstruction.

The automatic coil selection could be used instead of manual coil selection in conventional diagnostic imaging to avoid suboptimal coil selection and for further automation of the planning procedure, including for instance choosing the optimal phase encoding direction. The data, acquired with the selected coil subset, can be further reduced by applying one of the data compression methods proposed in [1,5]. The short selection time needed by the SVD-based coil selection makes it also applicable for various applications such as 2D real-time or interventional imaging, where the selection could be performed locally for each slice, enabling dynamical coil switching during image acquisition.

References

1. Buehrer M, Pruessmann KP, Boesiger P, Kozerke S (2007) Array compression for more efficient image reconstruction in MRI with large coil arrays. Magn Reson Med 57(6):1131–1139
2. Griswold MA, Jakob PM, Heidemann RM, Nittka M, Jellus V, Wang J, Kiefer B, Haase A (2002) Generalized autocalibrating partially parallel acquisitions (GRAPPA). Magn Reson Med 47(6):1202–1210
3. Guyon I, Elisseeff A (2003) An introduction to variable and feature selection. JMLR 3:1157–1182
4. Hardy CJ, Giaquinto RO, Piel JE, Rohling KW, Marinelli L, Fiveland EW, Rossi CJ, Park KJ, Darrow RD, Watkins RD, Foo TK (2007) 128-Channel body MRI with a flexible high-density receiver-coil array. In: Proceedings of the 15th annual meeting of ISMRM, Berlin, p 244
5. Huang F, Vijayakumar S, Akao J (2005) Software compression for partially parallel imaging with multi-channels. In: Proceedings of the 27th annual international conference of the

engineering in medicine and biology society. IEEE, Shanghai, pp 1348–1351
6. Kellman P, McVeigh ER (2005) Image reconstruction in SNR units: a general method for SNR measurement. Magn Reson Med 50(54):1439–1447
7. King SB, Varosi SM, Huang F, Duensing GR (2003) The MRI eigencoil: N channel SNR with N-receivers. In: Proceedings of the 11th annual meeting of ISMRM, Toronto, p 712
8. Lin FH, Wald LL, Ahlfors SP, Hamalainen MS, Kwong KK, Belliveau JW (2006) Dynamic magnetic resonance inverse imaging of human brain function. Magn Reson Med 56(4):787–802
9. Marinelli L, Hardy CJ (2007) Coil Selection optimization using mean-field annealing and its application to 128-channel imaging. In: Proceedings of the 15th annual meeting of ISMRM, Berlin, p 750
10. Mertins A (1999) Signal analysis: wavelets, filter banks, time-frequency transforms and applications. Wiley, New York
11. Mueller S, Umathum R, Speier P, Zühlsdorff S, Ley S, Semmler W, Bock M (2006) Dynamic coil selection for real-time imaging in interventional MRI. Magn Reson Med 56(5):1156–1162
12. Nehrke K, Börnert P, Mazurkewitz P, Winkelmann R, Grasslin I (2006) Free-breathing whole-heart coronary MR angiography on a clinical scanner in four minutes. J Magn Reson Imag 23(5):752–756
13. Niendorf T, Hardy CJ, Giaquinto RO, Gross P, Cline HE, Zhu Y, Kenwood G, Cohen S, Grant AK, Joshi S, Rofsky NM, Sodickson DK (2006) Toward single breath-hold whole-heart coverage coronary MRA using highly accelerated parallel imaging with a 32-channel MR system. Magn Reson Med 56(1):167–176
14. Ohliger AM, Grant AK, Sodickson DK (2003) Ultimate intrinsic signal-to-noise ratio for parallel MRI: electromagnetic field considerations. Magn Reson Med 50(5):1018–1030
15. Potthast A, Kalnischkies B, Kwapil G, Wald LL, Heumann T, Helmecke S, Schor S, Pirkl G, Buettner M, Schmitt M, Mattauch G, Hamm M, Stransky PB, Hebrank FX, Peyerl M (2007) A MRI system with 128 seamlessly integrated receive channels. In: Proceedings of the 15th annual meeting of ISMRM, Berlin, p 246
16. Press WH, Flannery BP, Teukolsky SA, Vetterling WT (1992) Numerical recipes in C: the art of scientific computing. Cambridge University Press, London
17. Pruessmann KP, Weiger M, Scheidegger MB, Boesiger P (1999) SENSE: sensitivity encoding for fast MRI. Magn Reson Med 42(5):952–962
18. Reeder SB, Wintersperger BJ, Dietrich O, Lanz T, Greiser A, Reiser MF, Glazer GM, Schoenberg SO (2005) Practical approaches to the evaluation of signal-to-noise ratio performance with parallel imaging: application with cardiac imaging and a 32-channel cardiac coil. Magn Reson Med 54(3):748–754
19. Reykowski A, Blasche M (2004) Mode matrix—a generalized signal combiner for parallel imaging arrays. In: Proceedings of the 12th annual meeting of ISMRM, Kyoto, p 1587
20. Roemer PB, Edelstein WA, Hayes CE, Souza SP, Mueller 0M (1990) The NMR phased array. Magn Reson Med 16(2):192–225
21. Siemens. Tim technical specifications 2007. http://www.cardiology.usa.siemens.com/products-and-it-systems/cardiology-products/magnetic-resonance/magnetom-avanto-with-tim/technical-specifications.aspx
22. Sodickson DK, Manning WJ (1997) Simultaneous acquisition of spatial harmonics (SMASH): fast imaging with radiofrequency coil arrays. Magn Reson Med 38(4):591–603
23. Winkelmann R, Börnert P, De Becker J, Hoogeveen R, Mazurkewitz P, Dössel O (2006) Dual-contrast single breath-hold 3D abdominal MR imaging. Magn Reson Mater Phy 19(6):297–304